Transcription–replication conflicts in primordial germ cells necessitate the Fanconi anemia pathway to safeguard genome stability

Yajuan Yang[a,b,c,d,e,f,g,1] 🔵, Weiwei Xu[a,b,c,d,e,1] 🔵, Fei Gao[h,i,1] 🔵, Canxin Wen[a,b,c,d,e], Simin Zhao[a,b,c,d,e], Yongze Yu[a,b,c,d,e], Wenlin Jiao[a,b,c,d,e], Xin Mi[a,b,c,d,e], Yingying Qin[a,b,c,d,e,2], Zi-Jiang Chen[a,b,c,d,e,j,k,l,2] 🔵, and Shidou Zhao[a,b,c,d,e,2]

Preserving a high degree of genome integrity and stability in germ cells is of utmost importance for reproduction and species propagation. However, the regulatory mechanisms of maintaining genome stability in the developing primordial germ cells (PGCs), in which rapid proliferation is coupled with global hypertranscription, remain largely unknown. Here, we find that mouse PGCs encounter a constitutively high frequency of transcription–replication conflicts (TRCs), which lead to R-loop accumulation and impose endogenous replication stress on PGCs. We further demonstrate that the Fanconi anemia (FA) pathway is activated by TRCs and has a central role in the coordination between replication and transcription in the rapidly proliferating PGCs, as disabling the FA pathway leads to TRC and R-loop accumulation, replication fork destabilization, increased DNA damage, dramatic loss of mitotically dividing mouse PGCs, and consequent sterility of both sexes. Overall, our findings uncover the unique source and resolving mechanism of endogenous replication stress during PGC proliferation, provide a biological explanation for reproductive defects in individuals with FA, and improve our understanding of the monitoring strategies for genome stability during germ cell development.

primordial germ cells | replication stress | transcription–replication conflicts | genome stability | Fanconi anemia pathway

Germ cells are responsible for faithfully transmitting genetic information across generations. In mammals, specification of primordial germ cells (PGCs) at the proximal posterior epiblast during early embryonic development marks the establishment of the germ cell lineage. Thereafter, PGCs migrate and colonize the developing genital ridge, where they undergo rapid proliferation via mitosis to establish a germ cell pool, which is a foundation for the reproductive reserve (1). Then, PGCs residing in the gonad are committed to gametogenesis, and mature gametes are subsequently produced through meiosis. Preserving germ cell genome with high fidelity during gametogenesis is paramount to the maintenance of a species. Elucidating the molecular basis that ensures germ cell genome stability would substantially facilitate our understanding of germline development and provide insights into reproductive aging and germline mutations.

The cell genome is constantly threatened by exogenous and endogenous DNA damage. The DNA damage response (DDR), a conserved mechanism that senses and removes DNA lesions, is essential for maintaining genome stability. The mutation rate is much lower in human and mouse germlines than that in somatic cells (2, 3), suggesting that the germ cells have superior ability to preserve genome stability. It is well established that efficient homologous recombination repair and rigorous surveillance by the CHK2-p63 pathway ensure the genome stability of oocytes during meiosis (4, 5). However, little is known about the underlying mechanisms for maintaining PGC genome stability during rapid mitosis. Interestingly, profound PGC developmental defects were observed in knockout mouse lines of ubiquitously expressed DNA repair factors, such as Fanconi anemia (FA) proteins, RAD54, MCM9, and ERCC1 (6–9), suggesting that compared with somatic cells, PGCs have an increased requirement for DNA repair ability to remove unique endogenous genome threats. However, the sources of endogenous DNA damage and responsible resolving mechanisms in PGCs remain largely unknown.

In the present study, we demonstrate that actively proliferating mouse PGCs sustain high levels of endogenous replication stress imposed by frequent transcription–replication conflicts (TRCs), which activate the FA pathway. The dual functions of R-loop resolution and replication fork (RF) stabilization underpin the necessity of the FA pathway in maintaining genome stability of PGCs in a challenging developmental stage.

Significance

Germ cells are capable of preserving their genetic information with high fidelity. We report that rapidly dividing mouse primordial germ cells (PGCs) are faced with high levels of endogenous replication stress due to frequent occurrence of transcription–replication conflicts (TRCs). Thus, PGCs have an increased requirement for the replication-coupled Fanconi anemia (FA) pathway to counteract TRC-induced replication stress, enabling their rapid proliferation to establish a sufficient reproductive reserve. This work provides insights into the unique genome feature of developing PGCs and helps to explain the reproductive defects in FA individuals.

[1]Y. Yang, W.X., and F.G. contributed equally to this work.

[2]To whom correspondence may be addressed. Email: qinyingying1006@163.com or chenzijiang@hotmail.com or shidouzhao@sdu.edu.cn.

Results

A High Frequency of TRCs Exists in Actively Proliferating PGCs.

Premeiotic PGCs undergo active proliferation—with a doubling time as short as about 12.6 h—and globally transcriptional up-regulation during mouse embryonic day (E)9.5~13.5 (10, 11). Consistently, E11.5 mouse PGCs exhibited an elevated transcriptional level evaluated by 5-ethynyl uridine (EU) incorporation assay in *Stella-EGFP* reporter mice (fourfold increase in PGC compared with soma; Fig. 1*A* and *SI Appendix,* Fig. S1) and immunostaining of RNA polymerase (Pol) II and its Ser2/5 phosphorylation (*SI Appendix,* Fig. S2*A*) and a higher proliferation rate evaluated by 5-ethynyl-2'-deoxyuridine (EdU) incorporation assay (45.4% in PGC vs. 20.9% in soma; Fig. 1*B*) and proliferating cell nuclear antigen (PCNA) immunostaining (*SI Appendix,* Fig. S2*B*). The global hypertranscription of PGCs may drive their rapid expansion. Nevertheless, when transcription and replication share a common DNA template, these two machineries inevitably encounter each other and TRCs are generated (12). As anticipated, colocalization of the transcription machinery (marked by RNA Pol II) and replication machinery (marked by PCNA) was observed in E11.5 PGCs using double immunofluorescence staining (*SI Appendix,* Fig. S2*C*). Furthermore, TRCs were determined by the proximity ligation assay (PLA) using antibodies against PCNA and RNA Pol II. The two primary antibodies that have bound to their targets in close proximity can be linked and then generate fluorescence foci, which indicate the occurrence of TRCs. In contrast with somatic cells, PGCs showed an approximately sixfold increase in PLA foci (Fig. 1*C*), indicating that PGCs had a high frequency of TRCs under an unperturbed developmental condition.

TRCs Impose High Levels of Endogenous Replication Stress on PGCs.

TRCs are considered as a major endogenous source of genome instability, which block replication progression by stalling the RFs and hinder the transcription process by promoting cotranscriptional R-loop formation (12–14). R-loop is a structure formed with a DNA–RNA hybrid and a displaced single-stranded DNA, which can act as a replication block (14). We were intrigued about whether such a high frequency of TRCs challenged the genome stability of PGCs. Indeed, PGCs harbored higher levels of R-loops recognized by the S9.6 antibody and γH2AX nuclear signals than those in somatic cells (Fig. 2*A*). Further analysis showed that the accumulation of γH2AX was observed in EdU-positive PGCs but not in EdU-negative PGCs (*SI Appendix,* Fig. S3*A*), indicating that the formation of γH2AX foci was associated with S-phase entry. Because γH2AX is a surrogate marker for both double-strand breaks (DSBs) and replication stress that refers to a condition where RF progression is impeded and the replication rate slows down (15–17), we wondered what kind of event γH2AX foci formation indicated in PGCs. In fact, γH2AX foci did not overlap with 53BP1 foci (*SI Appendix,* Fig. S3*B*), which is an alternative marker of DSBs, and their formation was mediated not by ataxia telangiectasia mutated (ATM) but rather by ATM and RAD3-related (ATR) (*SI Appendix,* Fig. S3 *C* and *F*), suggesting that there were high levels of replication stress in PGCs, and no DSBs were generated. Further, we also observed considerably increased expression of single-stranded DNA-binding proteins in PGCs, including RAD51 and RPA2, which are both involved in stalled RFs (*SI Appendix,* Fig. S3*D*). To directly assess the replication velocity, we cultured E11.5 genital ridges from *Stella-EGFP* reporter mice (*SI Appendix,* Fig. S1) and
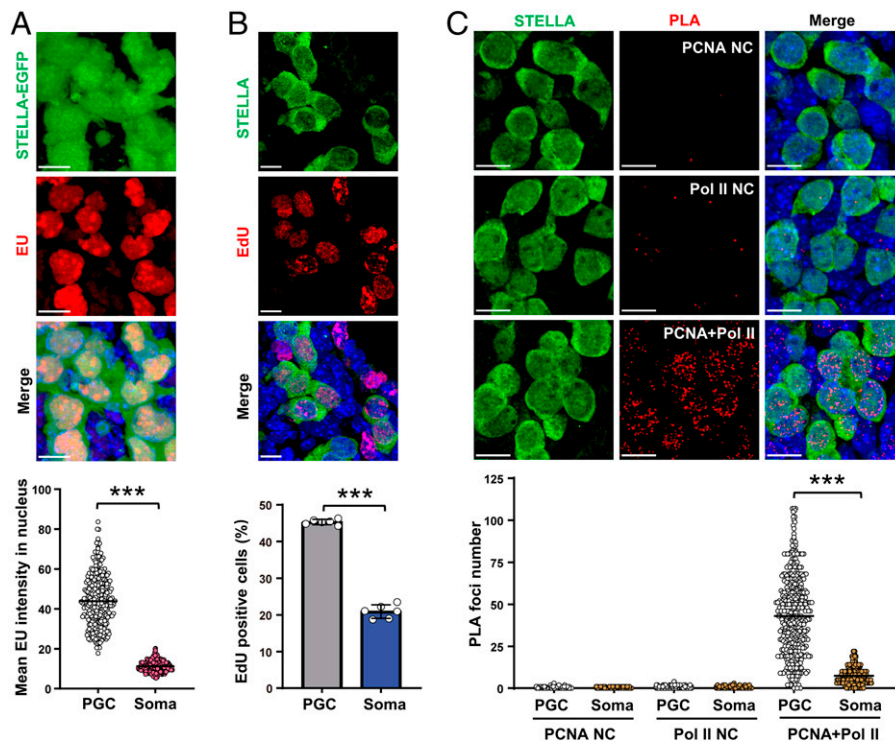

Fig. 1. A high transcriptional output and proliferation rate cause frequent TRCs in PGCs. (*A*) The transcriptional output was evaluated by EU incorporation in E11.5 genital ridges. *n* = 300/300 cells. (*B*) The proliferation rate was evaluated by EdU incorporation in E11.5 genital ridges. *n* = 6/6 embryos. (*C*) Representative images and enumeration of PCNA-Pol II PLA foci per nucleus in PGCs and somatic cells from E11.5 genital ridges. Staining for PCNA alone and Pol II alone served as single-antibody negative controls (NC). The individual red fluorescence focus represents a conflict event between replication and transcription machinery, and the foci number indicates TRC frequency. *n* = 300/300/300/300/300/300 cells. STELLA or STELLA-EGFP positivity indicates PGC, and STELLA negativity indicates soma. Data from individual embryos or cells are presented as dots; mean values (*A* and *C*) and the means ± SD (*B*) are marked. (Scale bars, 10 μm.) ***P < 0.001; unpaired two-tailed Student's *t* test (*A*–*C*).
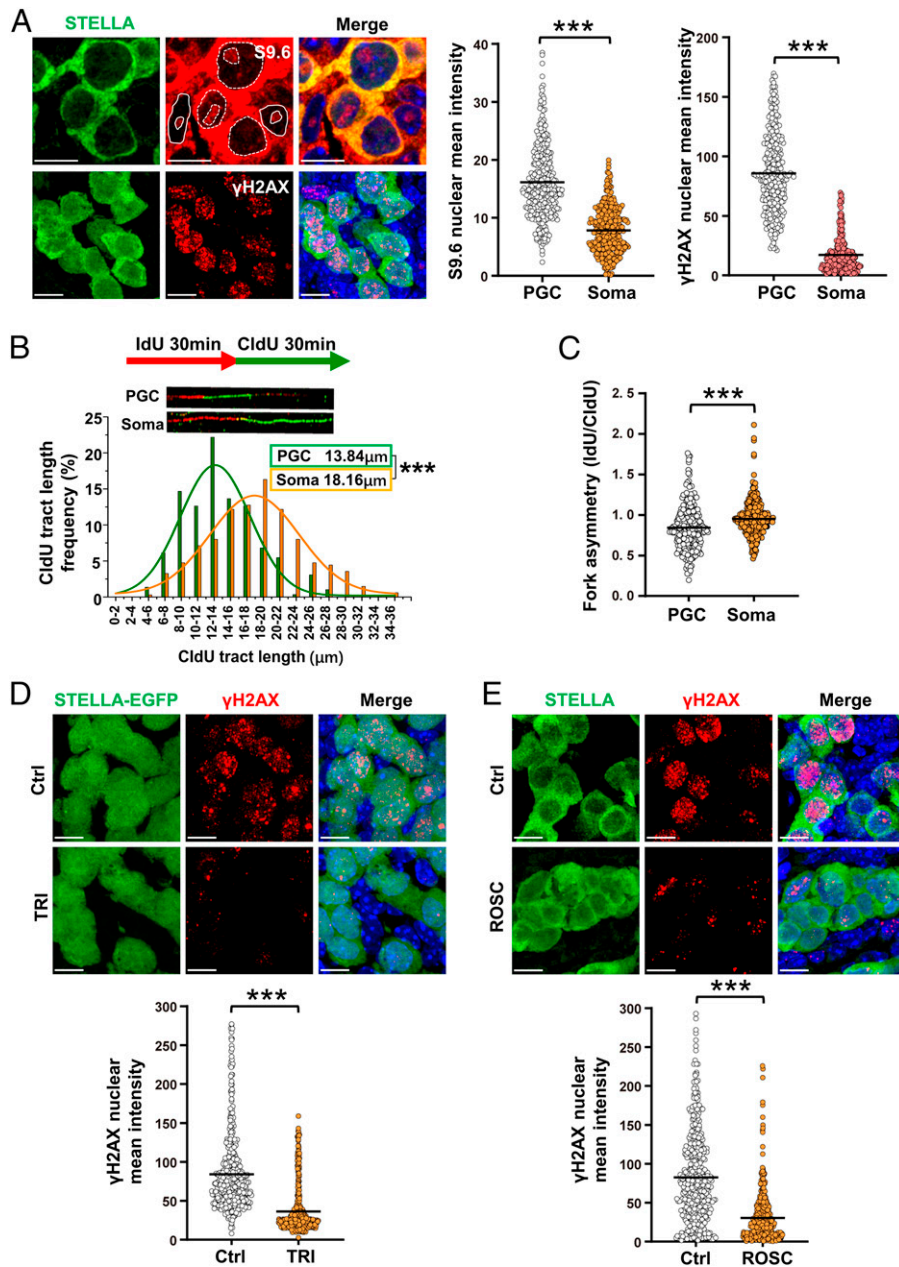
Fig. 2. A high frequency of TRCs imposes constitutive replication stress on PGCs. (*A*) Immunofluorescence staining and quantification of R-loop (recognized by the S9.6 antibody with signals in nucleolus excluded) and γH2AX nuclear signal (a marker for replication stress) intensity in E11.5 PGCs and somatic cells. *n* = 300/300/300/300 cells. (*B*) DNA fiber assay in FACS-sorted E11.5 PGCs and somatic cells, measuring the CldU track length (nascent DNA) to evaluate the velocity of RFs. *n* = 300/300 DNA fibers. (*C*) The IdU/CldU ratio was calculated to assess the asymmetry of RFs. *n* = 300/300 DNA fibers. (*D* and *E*) Representative images and mean fluorescence intensity quantification of γH2AX staining in E11.5 PGCs treated with a transcription inhibitor (TRI) for 3 h (*D*) or replication inhibitor (ROSC) for 8 h (*E*). *n* = 300/300/300/300 cells. STELLA or STELLA-EGFP positivity indicates PGC, and STELLA negativity indicates soma. Data from individual cells or DNA fibers are presented as dots, and the mean values are marked. Ctrl, control. (Scale bars, 10 μm.) ****P* < 0.001; unpaired two-tailed Student's *t* test (*A*–*E*).

consecutively pulse labeled active RFs with nucleotide analogs, iododeoxyuridine (IdU) and chlorodeoxyuridine (CldU), and then the newly synthesized DNA of sorted PGCs and somatic cells was visualized by immunofluorescence staining after DNA spreading (DNA fiber assay). Compared with somatic cells, reduced fork speed and increased asymmetry of RFs in PGCs were observed (Fig. 2 *B* and *C*). Collectively, these results indicate that actively proliferating PGCs harbor high levels of endogenous replication stress.

To investigate whether high levels of replication stress in PGCs originate from frequent TRCs, we next determined the relationship between γH2AX levels and replication and transcription progression. Although treating the cultured E11.5 genital ridges with the transcription inhibitor triptolide (TRI) did not perturb PGC proliferation (*SI Appendix*, Fig. S3 *E* and *F*), it remarkably reduced endogenous γH2AX levels (Fig. 2*D*), and inhibiting the replication of PGCs with roscovitine (ROSC) also significantly decreased γH2AX levels (Fig. 2*E* and *SI Appendix*, Fig. S3*F*). These data support γH2AX foci formation in PGCs being dependent on both replication and transcription progression. Collectively, these findings demonstrate that frequent TRCs disturb replication progression and impose high levels of endogenous replication stress on PGCs.

TRCs Activate the FA Pathway to Coordinate Replication and Transcription in PGCs. Although facing high levels of endogenous replication stress induced by TRCs, PGCs are still capable of preserving genome stability and undergo rapid cell cycle progression, indicating that PGCs are equipped with powerful replication-coupled mechanisms to resolve frequent TRCs and ensure faithful duplication of a challenging genome. The FA pathway, which is responsible for interstrand cross-link (ICL) repair, is also involved in resolving TRCs (12, 18, 19). Until now, in all 22 FA genes reported, 19 FA-null mouse models exhibit massive reduction of germ cells, and 8 of them (*Fanca, b, c, d2, l, m, g,* and *v*) have been found to exhibit PGC loss during the active proliferation stage (6, 20). This evidence strongly suggests that a functional FA pathway is essential for PGCs to survive the fast expansion period. Therefore, we hypothesize that the FA pathway plays a central role in protecting PGCs from TRC-induced genome instability.

To address this question, we first determined whether this pathway was activated in S-phase PGCs. The FA proteins are divided into three functional groups, including FA core complex, FANCI-FANCD2 complex, and downstream DNA repair proteins (21). The ubiquitination of FANCI-FANCD2 complex is a key event of the FA pathway activation and FANCD2 monoubiquitination or foci formation is often used to indicate the FA pathway activation (22). In contrast to somatic cells, PGCs showed high levels of FANCD2 protein and EdU-positive PGCs had a 10-fold increase in FANCD2 foci formation compared to EdU-positive somatic cells (Fig. 3*A*). In addition, FANCI, which is a binding partner and essential for ubiquitination of FANCD2 (23), was also highly expressed and colocalized with FANCD2 foci (Fig. 3*B*), further indicating that the FA pathway was strongly activated in unperturbed S-phase PGCs. Consistent with previous studies (24, 25), inhibition of ATR but not ATM reduced FANCD2 foci formation (Fig. 3*C*), demonstrating that ATR regulated the replication stress response and triggered the activation of the FA pathway in PGCs. Subsequently, we determined whether the FA pathway was active at TRC sites. The PLA results showed that FANCD2 colocalized with the replication apparatus (marked by PCNA) or transcription apparatus (marked by RNA Pol II) more frequently in PGCs than in somatic cells (Fig. 3*D*). Furthermore, inhibiting both transcription and replication significantly attenuated FANCD2 foci formation (Fig. 3 *E* and *F*). These results suggest that the FA pathway is constitutively activated by TRCs in PGCs.
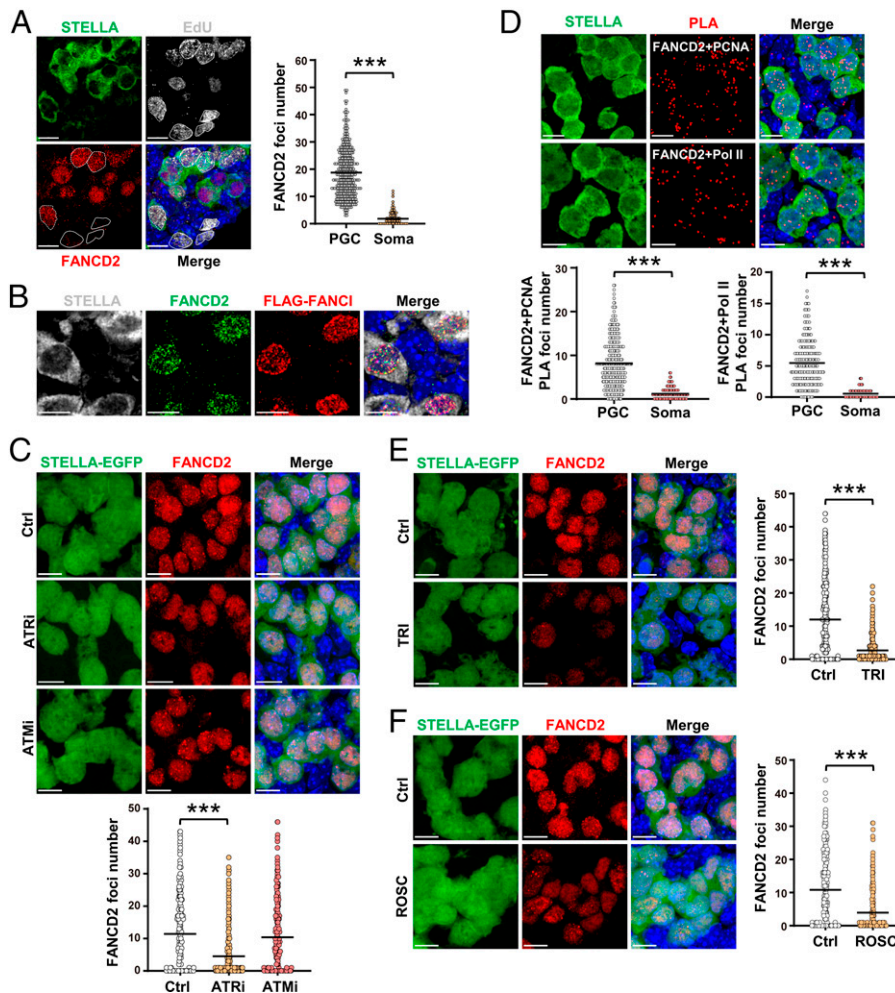

Fig. 3. TRCs activate the FA pathway in PGCs. (*A*) FANCD2 immunostaining and EdU incorporation in E11.5 genital ridges, and FANCD2 foci number was quantified in EdU-positive PGCs and somatic cells. *n*=300/300 cells. (*B*) Double immunostaining for FANCD2 and FLAG-FANCI in E11.5 genital ridges. (*C*) Immunostaining and quantification of FANCD2 foci in PGCs in cultured E11.5 genital ridges treated with an ATR inhibitor (ATRi) or ATM inhibitor (ATMi). *n* = 300/300/300 cells. (*D*) Representative images and quantification of FANCD2-PCNA PLA foci and FANCD2-Pol II PLA foci per nucleus in PGCs and somatic cells from E11.5 genital ridges. The red fluorescence foci indicate the location of the two target proteins in close proximity. *n* = 300/300/300/300 cells. (*E* and *F*) Representative images and quantification of FANCD2 foci in PGCs from cultured E11.5 genital ridges treated with transcription inhibitor (TRI) for 3 h (*E*) or replication inhibitor (ROSC) for 8 h (*F*). *n* = 300/300/300/300 cells. STELLA or STELLA-EGFP positivity denotes PGC; STELLA negative indicates soma. Data points from individual cells are presented as dots. The means are indicated (*A*, and *C–F*). (Scale bars, 10 μm.) Ctrl, control. ***P < 0.001; unpaired two-tailed Student's *t* test (*A*, and *C–F*).

To validate the role of the FA pathway in PGC development, we constructed a *Fanci* knockout (*Fanci*$^{-/-}$) mouse (26) and a *Fancd2* mutant mouse in which ubiquitination was disrupted as a result of the K559R substitution mutation (*SI Appendix*, Fig. *S4A*). PGCs in both mouse models failed to form FANCD2 foci (Fig. 4*A*); in addition, the expression of FANCD2 was decreased in *Fanci*$^{-/-}$ mouse embryonic fibroblasts (MEFs) and ubiquitinated FANCD2 was undetectable in *Fanci*$^{-/-}$ MEFs upon exposure to mitomycin (MMC) or aphidicolin (APH) —agents known to induce ICLs and replication stress, respectively (*SI Appendix*, Fig. *S6C*). These results demonstrate that FA pathway activation is abrogated in both mouse models.

Loss of FA pathway activity did not interfere with the global transcriptional level of PGCs (*SI Appendix*, Fig. *S7A*), but

resulted in a significant increase in TRC frequency and elevated levels of R-loops (Fig. 4 *B* and *C*). Furthermore, *Fanci*$^{-/-}$ MEFs showed increased TRC frequency, aberrant accumulation of R-loops, and decreased RF velocity (*SI Appendix*, Fig. *S5 A–E*); we subsequently found that removing R-loops via overexpression of RNase H1 reduced collisions between transcription and replication machinery and restored replication speed (*SI Appendix*, Fig. *S5 A–E*), suggesting that unscheduled accumulation of R-loops due to FA pathway disability exacerbated TRCs and hindered RF progression.

Stalled RFs need protection to prevent nascent DNA degradation and RF collapse (27). To elucidate the role of FANCI in the protection of RFs, we used APH to induce fork stalling in MEFs and assessed RF stability by DNA fiber assay. A significant
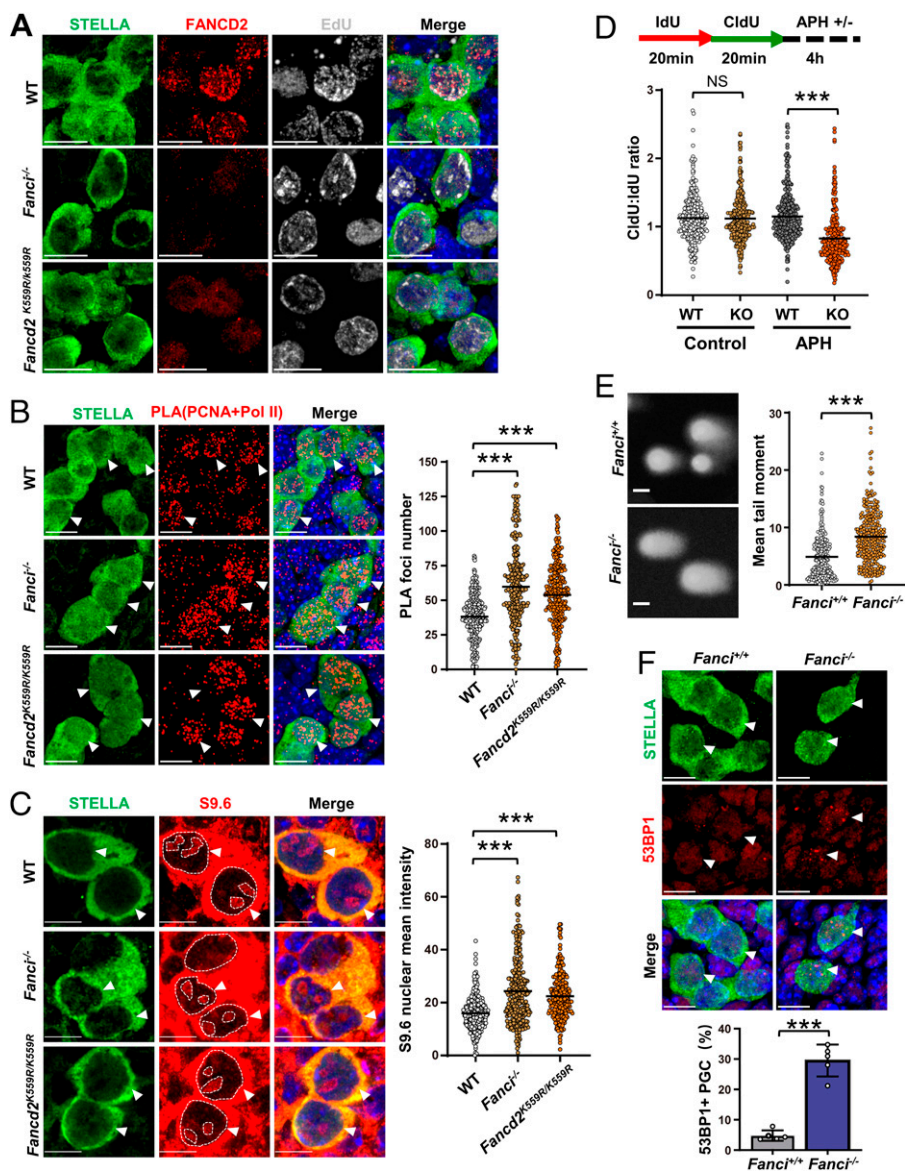

Fig. 4. FA pathway inactivation results in aggravated TRCs, R-loop accumulation, and DNA damage in PGCs. (*A*) Representative images of costaining with FANCD2 and EdU in wild-type, *Fanci*$^{-/-}$ and *Fancd2*$^{K559R/K559R}$ E11.5 genital ridges. (*B*) Representative images and quantification of PCNA-Pol II PLA foci per nucleus in wild-type, *Fanci*$^{-/-}$, and *Fancd2*$^{K559R/K559R}$ PGCs in E11.5 genital ridges. The quantification of red fluorescence foci indicates the TRC frequency. *n* = 300/300/300 cells. (*C*) Representative images and quantitation of R-loop nuclear signal intensity (recognized by the S9.6 antibody with signals in nucleolus excluded) in wild-type, *Fanci*$^{-/-}$, and *Fancd2*$^{K559R/K559R}$ PGCs from E11.5 genital ridges. *n* = 300/300/300 cells. (*D*) DNA fiber assay showing the ratio of CldU and IdU track length in wild-type and *Fanci*$^{-/-}$ MEFs treated with APH (1 μM) for the indicated times. *n* = 300/300/300/300 DNA fibers. (*E*) Neutral comet assay of E11.5 magnetic beads sorted wild-type and *Fanci*$^{-/-}$ PGCs. *n* = 400/400 nuclei. (*F*) Representative images of 53BP1 foci (DSB marker) and the percentage of 53BP1 foci-positive PGCs in E11.5 genital ridges. *n* = 5/5 embryos. STELLA positivity denotes PGC. WT, wild-type; KO, *Fanci*$^{-/-}$. Dots represent individual data points. The means (*B–E*) or means ± SD (*F*) are presented. (Scale bars, 10 μm.) Arrowheads indicate representative cells. NS, no significance, ***P < 0.001; unpaired two-tailed Student's *t* test (*B–F*).

increase in the resection of nascent DNA was observed in $Fanci^{-/-}$ MEFs, as shown by a decreased ratio of CldU and IdU tract length in the presence of APH (Fig. 4D), indicating that loss of FANCI resulted in instability of stalled RFs. Consistently, FANCD2 monoubiquitination was reported to be required for dissolving R-loops and stabilizing RFs (18, 28, 29). Collectively, these findings demonstrate that the FA pathway functions to resolve TRCs by removing R-loops and protecting stalled RFs in rapidly dividing PGCs.

Unrepaired DSBs in FA-Deficient Mice Cause PGC Proliferation Defects. A failure to resolve TRCs and stabilize stalled RFs results in fork collapse and formation of DSBs (13, 30), which are the most harmful type of DNA damage to cells. To evaluate the extent of DNA damage in PGCs, we enriched PGCs from E11.5 mouse genital ridges using SSEA-1 magnetic cell sorting and conducted the neutral comet assay. We found increased DNA damage content in PGCs from $Fanci^{-/-}$ embryos compared to wild-type embryos (Fig. 4E). Moreover, the percentage of PGCs that harbored nuclear foci of 53BP1 was significantly increased in E11.5 $Fanci^{-/-}$ embryos (Fig. 4F), suggesting that unrepaired DSBs accumulated in $Fanci^{-/-}$ PGCs. Consistently, compared to wild-type MEFs, $Fanci^{-/-}$ MEFs exhibited an extended olive tail moment (*SI Appendix*, Fig. S6A), increased proportion of 53BP1 foci-positive cells (*SI Appendix*, Fig. S6B), elevated levels of RPA2-s4/8 phosphorylation (*SI Appendix*, Fig. S6C), and an increased proportion of cells with micronuclei formation (*SI Appendix*, Fig. S6D) after treatment with MMC or the replication stress inducers APH and/or hydroxyurea (HU). These findings imply that FA pathway inactivation causes a defective response to replication stress and augments genome instability.

To systematically assess the impact of FA pathway inactivation on PGC development, we examined the expansion of the PGC population at various time points during gestation in both $Fanci^{-/-}$ and Fancd2 mutant mice. We found that the PGC numbers in E8.5 $Fanci^{-/-}$ and Fancd2 mutant embryos were comparable to those of their wild-type counterparts (Fig. 5A and *SI Appendix*, Fig. S4B), suggesting that specification of PGCs occurred normally. However, the PGC population in both $Fanci^{-/-}$ and Fancd2 mutant embryos was slightly decreased at E9.5 and dramatically reduced at E11.5 (Fig. 5A and *SI Appendix*, Fig. S4B), indicating that FA pathway inactivation resulted in severe loss of PGCs during the rapid proliferation window. Intriguingly, at E9.5, PGCs undergo a transition from relative hypoproliferation and transcriptional quiescence to hyperproliferation and hypertranscription states (10, 31). This evidence supports the specific time of PGC loss in FA-deficient embryos coinciding with the time when the physiological TRC frequency increases.

To further determine the cause of PGC depletion, we examined the cell cycle progression and apoptosis of PGCs. As with the wild-type PGCs, all $Fanci^{-/-}$ PGCs at E11.5 were positive for Ki67 staining (*SI Appendix*, Fig. S7B), indicating that $Fanci^{-/-}$ PGCs did not exit the cell cycle. Then, we combined EdU incorporation and cyclin B1 staining to analyze the mitotic cell cycle progression of PGCs. The results showed that deletion of FANCI led to a significantly decreased proportion of S-phase PGCs and an increased proportion of G2-phase PGCs (Fig. 5B), indicating that knockout of Fanci resulted in proliferation defects and cell cycle arrest of PGCs. Additionally, apoptosis was also enhanced in $Fanci^{-/-}$ PGCs, as indicated by increased cleaved-PARP1 staining, but the absolute number of apoptotic PGCs was fewer than 10 per embryo (Fig. 5C),

suggesting that increased apoptosis played a minor role in PGC loss of $Fanci^{-/-}$ embryos.

To shed light on the mechanism of PGC-related developmental defects, the consequence of DNA lesions in PGCs with FA pathway deficiency were further investigated. When DNA lesions occur, cells activate the DDR and cell cycle checkpoints to ensure accurate DNA duplication as well as ordered cell cycle progression (32). The p53 protein plays a key role in response to DNA damage and cell cycle checkpoint, and hyperactivated p53 has been linked to hemopoietic stem cell (HSC) attrition and PGC loss in FA-null mice (33, 34). Similarly, we found that $Fanci^{-/-}$ PGCs and MEFs treated with MMC or APH showed increased levels of phosphorylated p53 (Fig. 5D and *SI Appendix*, Fig. S6C), suggesting that p53 responded to replication stress-induced DNA damage. p53 is involved in both G1–S and G2–M cell cycle checkpoints (35), but PGCs lack the G1–S checkpoint (36). We therefore propose that DNA damage induced by FA pathway inactivation initiates the G2–M checkpoint and that activated p53 signaling triggers G2-phase arrest of PGCs. The extended G2 phase allows more time for DNA damage repair but leads to a dramatic loss of PGCs within the limited proliferation period. As expected, deletion of p53 partially rescued the PGC loss in $Fanci^{-/-}$ mice (Fig. 5E), validating that p53 could prevent damaged PGCs from expanding and transmitting detrimental genetic information.

The Functional FA Pathway Is Required for PGC Development and Normal Fertility. To further understand the role of the FA pathway in PGC development, the detailed phenotype of $Fanci^{-/-}$ mice was analyzed. PGCs experience genome-wide epigenetic reprogramming following their specification (37). Hence, we interrogated whether key events in this process occurred normally in $Fanci^{-/-}$ PGCs. We found that the epigenetic modifications, including 5-methylcytosine (5mC), histone H3 lysine 9 dimethylation (H3K9me2), and histone H3 lysine 27 trimethylation (H3K27me3), were removed or established normally in E11.5 $Fanci^{-/-}$ PGCs (*SI Appendix*, Fig. S7 C–E). Although the number was significantly reduced, the remnant PGCs could differentiate into few spermatogonia and oogonia, and the development of granulosa cells in the ovary and Sertoli cells in the testis was not affected in $Fanci^{-/-}$ mice (*SI Appendix*, Fig. S8A). However, deletion of FANCI and deficiency of ubiquitinated FANCD2 both led to complete follicle depletion in the ovaries in adult female mice and a massive loss of spermatogenic cells and sperm in the testis and epididymis, respectively, in adult male mice (Fig. 5F and *SI Appendix*, Fig. S4C). As a result, both female and male adult $Fanci^{-/-}$ mice were sterile (*SI Appendix*, Fig. S8B).

The FA proteins are expressed ubiquitously, and FA individuals usually show systemic phenotypes characterized by congenital abnormalities, progressive bone marrow failure, and predisposition to cancer (20, 38). But FA-deficient mice usually have a very limited, even no FA-related somatic phenotypes. In this study, $Fanci^{-/-}$ mice were born in expected Mendelian ratios in the progenies when $Fanci^{+/-}$ females mated with $Fanci^{+/-}$ males (*SI Appendix*, Fig. S8C), and no gross abnormalities in the appearance and growth of $Fanci^{-/-}$ mice were observed (*SI Appendix*, Fig. S8D) (26). These findings are inconsistent with a previous study, which reported a more severe systemic phenotype of $Fanci^{-/-}$ mice that recapitulated a FA phenotype (39). These distinct findings suggest that a functional FA pathway is specifically required for the development of PGCs but not somatic cells in the context of the mixed-background mouse strain we used.
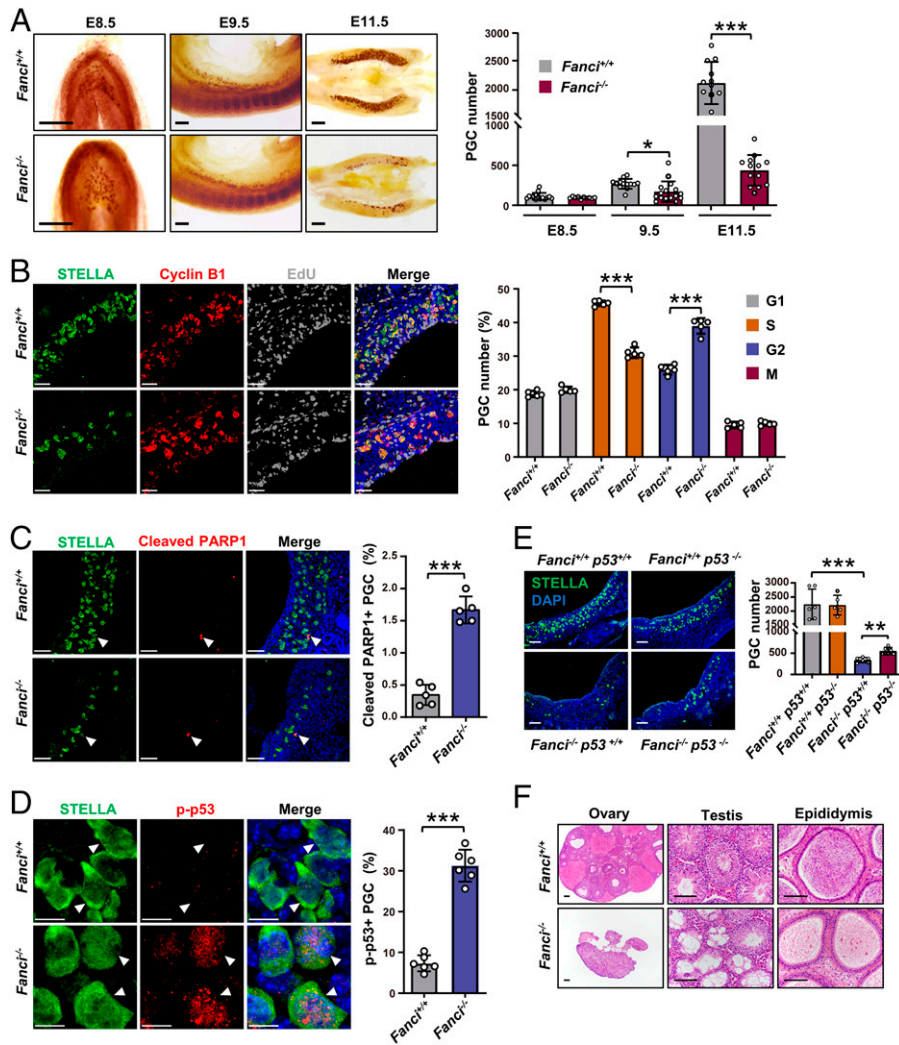
Fig. 5. The FA pathway is indispensable for PGC proliferation and fertility. (*A*) Alkaline phosphatase staining of whole-mount or genital ridges from wild-type and *Fanci⁻/⁻* mice and PGC counts at various embryonic stages as indicated. The reddish-brown spots indicate PGCs. $n = 15/10/13/16/12/14$ embryos. (*B*) Immunofluorescence staining of cyclin B1 and EdU incorporation in E11.5 wild-type and *Fanci⁻/⁻* genital ridges to evaluate the cell cycle progression of PGCs (G1, cyclin B1 negative; S, EdU positive; G2, cyclin B1 strongly positive in cytoplasm; M, cyclin B1 accumulation in the nucleus). $n = 5/5$ embryos. (*C*) Cleaved PARP1 immunostaining (an apoptotic marker) in E11.5 wild-type and *Fanci⁻/⁻* genital ridges to evaluate the apoptotic PGCs (STELLA and cleaved PARP1 double positive). $n = 5/5$ embryos. (*D*) Representative images of p-p53 immunostaining and quantification of the percentage of p-p53–positive PGCs in E11.5 genital ridges from wild-type and *Fanci⁻/⁻* embryos. $n = 6/6$ embryos. (*E*) Deletion of p53 to rescue the reduction in the number of PGCs in E11.5 *Fanci⁻/⁻* embryos. STELLA immunostaining to quantify the PGC number in the genital ridges with the indicated genotypes. $n = 6/5/6/6$ embryos. (*F*) Hematoxylin and eosin staining of wild-type and *Fanci⁻/⁻* paraffin sections of ovaries from 12-wk-old females and testes and epididymis from 10-wk-old males. Alkaline phosphatase staining or STELLA positivity indicates PGC. Data points from individual embryos are presented as dots. Data are presented as the means ± SD (*A–E*). (Scale bars, 200 μm in *A*; 50 μm in *B, C, E*, and *F*; and 10 μm in *D*.) Arrowheads indicate representative cells. *$P < 0.05$, **$P < 0.01$, ***$P < 0.001$; unpaired two-tailed Student's t test (*A–E*).

Apart from PGC deficiency, meiotic defects have also been detected in some FA mutant mice (6, 39). To dissect the independent function of FANCI in germ cell development at different stages, we conditionally deleted *Fanci* in PGCs and meiotic germ cells by using a *Blimp1-Cre–* and *Stra8-GFPCre–*mediated recombination strategy, respectively (*SI Appendix*, Fig. S9 *A–C*). In line with the phenotype of global knockout mice, *Fanci^fl/-^;Blimp1-Cre* mice also showed profound developmental defects of PGCs as well as subsequent germ cells (*SI Appendix*, Fig. S9 *D* and *E*). However, no obvious abnormalities were observed in ovary and testis morphology (*SI Appendix*, Fig. S9F), and meiotic prophase I progression of spermatocytes and oocytes in *Fanci^fl/-^;Stra8-GFPCre* mice (*SI Appendix*, Fig. S9 *G–I*). Besides, both female and male *Fanci^fl/-^;Stra8-GFPCre* mice were fertile, suggesting that the FA pathway was not essential for meiosis. Taken together, our findings demonstrate that the failure to resolve TRC-induced endogenous replication stress in rapidly dividing PGCs underlies the compromised fertility in FA-null mice and individuals.

Discussion

Rapid cell cycle progression and hypertranscription threaten genome stability and contribute to tumorigenesis by causing endogenous replication stress (40, 41). Interestingly, developing PGCs endure fast proliferation and global up-regulation of transcriptional output without interference with their genome stability. However, little is known about how PGCs preserve genetic information with high fidelity. In the present study, we report that the rapidly proliferating PGCs encounter high levels of endogenous replication stress induced by TRCs and demonstrate that the crucial role of the FA pathway in resolving TRCs enables PGCs to maintain genome stability during their active proliferation stage.

To reduce TRCs, transcription and replication progressions are usually separated spatially and temporally, and tend to proceed in a codirectional orientation (12). In this study, we found that increased transcription activity resulted in frequent TRCs and consequent high levels of replication stress in rapidly proliferating PGCs (Figs. 1C and 2 A–C). Active transcription redistributes replication origins in G1 phase to reduce TRCs, but rapid cycling cells shorten G1 phase and thus leave insufficient time to coordinate transcription and replication (12). In addition, elevated RNA Pol II loading on the DNA template increases transcription roadblocks to the replisome (*SI Appendix*, Fig. S2A). Therefore, frequent TRCs cannot be avoided when hyperproliferation couples with hypertranscription (Fig. 1C). This feature makes PGCs dependent on the FA proteins to maintain their genome stability. As a result, the endogenous DNA damage due to unresolved TRCs led to FA-related proliferation defects of PGCs (Figs. 4 B, E, and F and 5B). Similarly, a profound HSC defect was observed in both human and murine FA fetuses during the stage of rapid expansion (42), and accumulation of proliferation-induced DNA damage caused the attrition of HSCs in FA-deficient individuals and mice (43). Additionally, gerneration of induced pluripotent stem cells (iPSCs) from FA-null somatic cells was inefficient, owing to a failure to overcome endogenous DNA damage (44, 45). HSCs and iPSCs also globally up-regulate transcriptional output to fuel their rapid proliferation (46). Thus, an inablity to resolve replication stress induced by increased TRCs may also, at least partially, explain the replication-related DNA damage in FA-null stem cells.

The PGC pool is the basis for gametogenesis and a fundamental determinant of the reproductive reserve. In agreement with FA-null mouse models, the fertility of FA individuals is severely impaired, manifesting as premature ovarian insufficiency (POI) in females and as nonobstructive azoospermia (NOA) in males (6). Recently, many FA gene mutations have been identified in isolated POI and NOA patients and the FA pathway has been reported to be associated with female reproductive lifespan in humans (47, 48). Our results offer a mechanistic basis by elucidating that this pathway overcomes high replication stress imposed by TRCs and maintains genome stability in actively proliferating PGCs, ultimately ensuring the establishment of sufficient reproductive reserve.

In this study, although we evaluate TRCs in PGCs in situ by using the PLA assay with anti-PCNA and anti-RNA Pol II antibodies, the localization and signature of TRCs across PGC genome need to be further characterized. In addition, genetic ablation of p53 only partially restored the PGC population in FA-null mice, suggesting that there were additional mechanisms to restrict the spread of damaged PGCs.

In summary, we reveal that high levels of endogenous replication stress induced by frequent TRCs necessitate a functional FA pathway to protect genome stability during the rapid proliferation period of PGCs. Disabling the FA pathway results in DNA damage derived from a failure to resolve R-loops and protect stalled RFs, and the proliferation defects of PGCs ultimately impair fertility (Fig. 6). Our findings provide an explanation for the common infertility feature in FA-null mice and FA patients and give insight into the endogenous genome threats and corresponding strategies that safeguard genome stability in developing PGCs.

Materials and Methods

Animals. All animal experiments were performed in accordance with the ethical guidelines approved by the animal care and research committee of Shandong
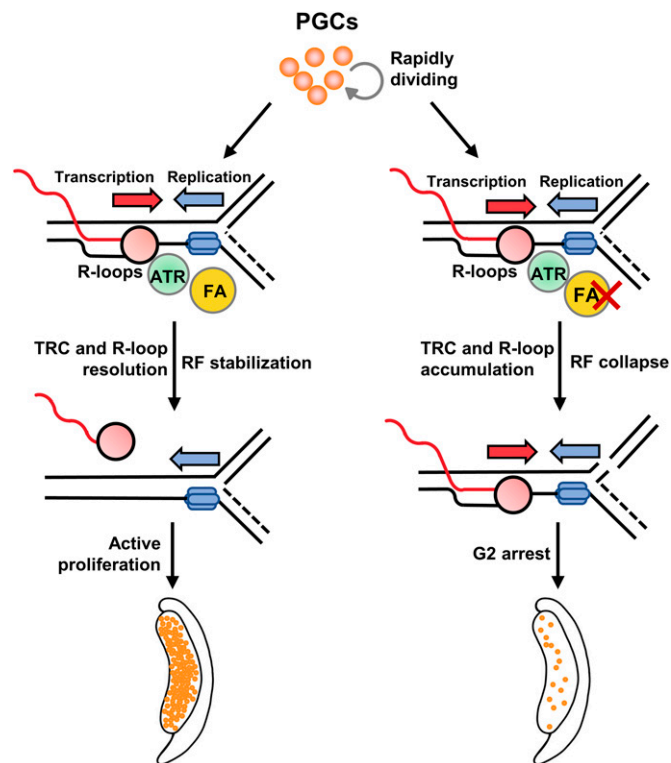

Fig. 6. The working model of how the FA pathway orchestrates PGC development. PGCs encounter frequent TRCs during rapid division, and TRCs impede replication and transcription progression, causing frequent RF stalling and R-loop accumulation. Consequently, ATR kinase activates the FA pathway to handle TRCs and R-loops and stabilize stalled RFs. The obstacle is removed and forks restart following FA pathway activation to ensure faithful replication of genome, thus maintaining PGC genome stability during their active proliferation stage. When the FA pathway is disrupted, a failure to resolve TRCs and R-loops in a timely manner and destabilization of stalled forks result in fork collapse and DNA damage. The accumulation of DNA damage activates p53 signaling to trigger G2-phase arrest of PGCs. Prolonged G2 phase impairs cell expansion and ultimately leads to a dramatic loss of PGCs.

University. Mice were raised in individually ventilated cages under specific pathogen-free conditions. Wild-type mice were purchased from Beijing Vital River Laboratory Animal Technology Co., Ltd. *Stella-EGFP* reporter mice were created by inserting an HA tag-P2A-EGFP sequence before the stop codon of the *Stella* gene, and EGFP protein expression indicated PGCs (*SI Appendix*, Fig. S1 A and B). EGFP successfully marked PGCs beginning at E8.5, and the fertility of homozygous female mice was normal (*SI Appendix*, Fig. S1 C–E). *Fanci*$^{-/-}$ mice with a 98-bp deletion in exon 5 of the *Fanci* locus were generated by Nanjing Sync Biotech using CRISPR-Cas9 technology (26). *Fancd2*^{K559R} mutant mice possessed a mutation that disrupted monoubiquitylation. The *p53*$^{-/-}$ mice were obtained by targeted deletion of exon 3 to exon 9. *Flag-Fanci* mice with a 3× Flag sequence behind the start codon of *Fanci* were generated to label FANCI protein expression (26). *Fanci-Flox* mice had two Loxp sites flanking exon 3 of the *Fanci* gene. *Stella-EGFP*, *Fancd2*^{K559R}, and *p53*$^{-/-}$ mice were obtained from Cyagen Bioscience. *Flag-Fanci* mice and *Fanci-Flox* mice were generated using CRISPR-Cas9 technology. *Blimp1-Cre* mice were obtained from The Jackson Laboratories. *Stra8-GFPCre* mice were a generous gift from Prof. Ming-Han Tong at the Chinese Academy of Sciences (49). All mice generated by CRISPR-Cas9 technology were derived from C57BL/6 mice and then crossed with ICR mice. The sequences of PCR primers used for genotyping are listed in *SI Appendix*, Table S1.

Genital Ridge Culture. Wild-type female ICR mice were mated with homozygous *Stella-EGFP* male mice. Noon of the day when vaginal plugs of mated females were observed was considered as E0.5. Pregnant female mice were killed at E11.5, and genital ridges were carefully dissected under a stereoscope and collected in cold Leibovitz's L-15 medium supplied with 10% foetal bovine serum

(FBS) and 1% streptomycin/penicillin. The genital ridges were washed three times with culture medium (MEMα + 10% KnockOut Serum Replacement + 1.5 μM 2-O-α-D-glucopyranosyl-L-ascorbic acid + 1% streptomycin/penicillin) (50). Thereafter, genital ridges were cultured in six-well plates using medium with the corresponding inhibitors for the appropriate times (ATRi VE-821, 10 μM for 4 h; ATMi Ku60019, 5 μM for 4 h; triptolide 0.25 μM for 3 h; and roscovitine 50 μM for 8 h) in a 37 °C incubator with 5% CO_2. Then, cultured genital ridges were fixed with 4% paraformaldehyde (PFA) for 1 h at room temperature, washed three times with phosphate buffer saline (PBS), and embedded in optimal cutting temperature (OCT) compound. The genital ridges were then utilized for frozen sectioning and immunofluorescence staining.

Immunostaining and Confocal Microscopic Analysis. Embryos from pregnant female mice at E11.5 were collected and fixed with 4% PFA overnight at 4 °C. After fixation, the embryos were washed three times with PBS, and genital ridges were dissected and embedded in OCT compound. The tissues were sectioned at 10 μm on a freezing microtome and mounted on adhesion slides. The slides were immersed in PBS to remove the OCT compound. The samples were permeabilized and blocked via incubation with 0.3% Triton X-100 containing 10% bovine serum albumin (BSA) or donkey serum for 1 h at room temperature. Samples were incubated at 4 °C overnight with appropriate primary antibodies (*SI Appendix*, Table S2) diluted in 1% BSA containing 0.3% Triton X-100. Subsequently, slides were washed with PBS containing 0.1% Triton X-100 (PBST) three times and then incubated with Alexa Fluor conjugated secondary antibodies diluted in PBST containing 5 μg/mL Hoechst 33342 for 1 h at room temperature. Finally, the slides were washed three times with PBST and mounted with antifade reagent. Immunofluorescence images were captured through a z axis scan with an interval of 1∼2 μm on a confocal microscope (ANDOR Technology). The intensity of nuclear RNA Pol II, γH2AX, S9.6, and FANCD2 staining was quantitated using ImageJ software.

EdU Incorporation Assay. Pregnant mice (E11.5) were intraperitoneally injected with 100 mg/kg EdU solution. After 1 h, the injected mice were killed. The embryos were collected and fixed with 4% PFA at 4 °C overnight. The genital ridges were dissected, embedded in OCT compound, and sectioned at a thickness of 10 μm. Samples were washed three times in PBS, incubated with 2 mg/mL glycine solution for 10 min, permeabilized twice with 0.5% Triton X-100 for 10 min, and incubated with EdU reaction buffer prepared according to the manufacturer's instructions (Ribo Bioscience) for 30 min at room temperature. Thereafter, samples were labeled with STELLA antibody following a standard immunofluorescence procedure and counterstained with Hoechst 33342. Images were captured with a confocal microscope (ANDOR Technology), and the EdU-positive cells were counted manually.

EU Incorporation Assay. To assess global RNA synthesis, we labeled cultured genital ridges from *Stella-EGFP* reporter mice with 1 μM EU for 1 h. Tissues were then fixed with 4% PFA for 1 h at room temperature, embedded in OCT compound, and sectioned at a thickness of 10 μm. Sections were washed with PBS, permeabilized once with 0.5% Triton X-100 for 15 min, and incubated with a Click-iT EU reaction mixture for 30 min, prepared according to the manufacturer's instructions (Invitrogen, C10330). Finally, sections were washed once with Click-iT reaction rinse buffer, and nuclei were counterstained with Hoechst 33342. Images were acquired immediately after the procedure was completed.

Generation of Primary MEFs. Pregnant mice were killed at E12.5∼E13.5. All the embryos were collected, and a small piece of tissue was excised from each embryo for genotyping. After the limbs, tail, viscera, and head of the embryos were removed, the trunks were collected and fragmented with sharp scissors. The fragmented tissues were digested for 4 min in a 37 °C water bath with 0.05% trypsin (Invitrogen) to dissociate into a single-cell suspension. Cells were collected by centrifugation at 1,000 rpm for 5 min and cultured in Dulbecco's modified eagle medium (DMEM) with 10% FBS and 1% streptomycin/penicillin.

PLA. For the PLA in genital ridges, E11.5 embryos were fixed with 4% PFA overnight at 4 °C and washed on a shaker with PBS three times. Genital ridges were dissected carefully, dehydrated in degraded alcohol, embedded in paraffin, and cut into sections with a thickness of 7 μm. Sections were deparaffinized in xylene, rehydrated in a series of degraded alcohols, boiled for 20 min in citrate buffer (pH 6.0) for antigen retrieval, blocked, and penetrated for 1 h at room temperature with 10% donkey serum containing 0.3% Triton X-100. Tissues

were then incubated with appropriate primary antibodies at 4 °C overnight. Sections were washed three times in PBST, incubated in PLA probe solution containing anti-mouse plus and anti-rabbit minus for 1 h at 37 °C, washed twice in washing buffer A (Sigma), and incubated in a ligation solution for 30 min at 37 °C. Duolink In Situ Detection Reagents (Red, Sigma) were prepared according to the manufacturer's instructions, and the sections were incubated with premixed detection reagents for 100 min at 37 °C. Sections were washed twice with washing buffer A, washed once with 0.01× washing buffer B, and subjected to immunostaining using an anti-STELLA antibody to label PGCs. Finally, nuclei were counterstained with Hoechst 33342 for 30 min. Slides were mounted in antifade reagent and imaged under a confocal microscope. The fluorescence foci indicate the location of the tested proteins in close proximity.

In preparation for the PLA in MEFs, cells were seeded onto coverslips before they were fixed with 4% PFA for 15 min at room temperature, washed three times with PBS, penetrated with cold methanol for 10 min at −20 °C, washed with distilled water three times, blocked for 1 h at room temperature using 10% donkey serum with 0.3% Triton X-100, and then incubated with RNA Pol II antibody and PCNA antibody overnight at 4 °C. The remnant procedures for Duolink In Situ Detection were performed as described above.

DNA Fiber Assay. For the DNA fiber assay in sorted PGCs and somatic cells, wild-type ICR pregnant females that were mated with homozygous *Stella-EGFP* male mice were killed at E11.5. The genital ridges were collected and cultured as described above in *Genital Ridge Culture*. The cultured genital ridges were sequentially pulse labeled with 50 μM IdU (Sigma) and 250 μM CldU (Sigma) for 30 min. The labeled genital ridges were incubated with Accutase (Thermo Fisher) for 25 min at 37 °C to disperse into single cells. Digestion was stopped by adding excessive Leibovitz's L-15 medium supplied with 10% FBS. The cell suspension was filtered through a 70-μm mesh from SmartStrainers (Milteny Biotech), centrifuged for 8 min at 300 × g at 4 °C, and resuspended in 0.5% BSA. The cells were immediately subjected to fluorescence activated cell sorting (FACS) (BD FACSAria III) for EGFP-positive cells (PGCs) and EGFP-negative cells (somatic cells). The sorted PGCs and somatic cells were pelleted by centrifugation for 8 min at 300 × g at 4 °C and resuspended at a concentration of 5 × 10^5∼1 × 10^6 cells/mL in cold PBS. Two microliters of the cell suspension were spotted onto one end of the adhesion glass slide. After the samples were air dried for 3 min at room temperature, 12 μL of lysis buffer (50 mM ethylene diamine tetraacetic acid tetrasodium (EDTA) and 0.5% sodium dodecyl sulfonate in 200 mM Tris·HCl, pH 7.5) was added to the top of the cell suspension. The solution was gently stirred with the pipette tip to mix the solutions and lyse the cells. The slides were then tilted to 15°∼45° to make the liquid flow to the other end slowly, and then slides were placed at an angle of 30°∼45°. The slides were completely air dried and fixed with methanol/acetic acid (volume ratio 3:1) for 10 min. The slides were washed in distilled water twice, degenerated in 2 N HCl for 60 min at room temperature, incubated with anti-BrdU antibodies (rat and mouse), and subjected to standard immunofluorescence procedures (51). DNA fiber images were acquired with a confocal microscope.

For the DNA fiber assay in MEFs, cells were obtained as described above. MEFs were consecutively pulsed with 25 μM IdU and 250 μM CldU for the appropriate duration. Then, MEFs were digested and resuspended at a concentration of 5 × 10^5∼1 × 10^6 cells/mL in cold PBS. The DNA fiber assay procedures were conducted as described above.

Magnetic PGC Sorting. After mated with *Fanci*$^{+/−}$ males, pregnant *Fanci*$^{+/−}$ female mice were killed at E11.5, and the genital ridges of each embryo were collected in cold Leibovitz's L-15 medium. A small piece of tissue was used for quick genotyping utilizing the KAPA Mouse Genotyping Kit (Sigma). The wild-type or *Fanci*$^{−/−}$ genital ridges were pooled and digested into a single-cell suspension as described above in the *DNA Fiber Assay*. The cell pellets were resuspended in 80 μL of DPBS containing 0.5% BSA and 2 mM EDTA (buffer), after which 20 μL of anti-SSEA-1 microbeads were added to the cell suspension, mixed well, and incubated at 4 °C for 15 min in the refrigerator. Then, the cells were washed once and centrifuged at 300 × g for 8 min at 4 °C. The cell pellets were resuspended in 500 μL of the buffer.

The separation columns were placed in the magnetic field of the separator and rinsed with 500 μL of the buffer. A 500-μL cell suspension was applied to the column, and the flow-through contained somatic cells (unlabeled cells). The

columns were washed with 500 μL of the buffer three times, removed, placed onto a collection tube, and immediately added to 500 μL of the buffer. The magnetically labeled cells (SSEA1-positive cells, PGCs) were flushed out by pushing the plunger into the column quickly. The magnetic-positive cells were centrifuged at $300 \times g$ for 8 min at 4 °C and resuspended at a concentration of 1×10^6 cells/mL in cold DPBS. The positive cells were used for the neutral comet assay.

Neutral Comet Assay. A neutral comet assay for magnetic beads sorted PGCs or MEFs was conducted as described with minor modifications (52). Briefly, 80 μL of melted 0.8% agarose (Sangon Biotech) was dropped onto glass slides and spread with a coverslip, and the slides were dried in a 37 °C incubator. Ten microliters of sorted PGC suspension or MEFs at a cell density of 1×10^6 cells/mL were mixed with 70 μL of low-melting temperature 0.8% agarose (Sangon Biotech). Ten microliters of the cell-agarose mixture was pipetted and spread onto the prepared glass slide immediately by using a coverslip. The slides were then stored at 4 °C for 15 min to allow solidification before they were immersed in neutral lysis buffer (2.5 M NaCl, 100 mM Na$_2$ EDTA, 10 mM Tris, 1% N-lauroylsarcosine, and 1% Triton X-100 [pH 9.5]) for 1 h at room temperature after removing the coverslip. The slides were washed three times with ddH$_2$O and submerged in neutral electrophoresis buffer (300 mM sodium acetate, 100 mM Tris [pH 8.3]) for 30 min. Electrophoresis was conducted at a current of 80 mA and a voltage of 20 V for 20 min. After electrophoresis, the slides were washed with ddH$_2$O three times, fixed with 100% ethanol, and air dried overnight at room temperature. The slides were rinsed with ddH$_2$O and counterstained with Hoechst 33342 for 30 min at room temperature. Slides were mounted with antifade reagent and viewed under a fluorescence microscope (Olympus BX53). The olive tail moments were analyzed using CASP comet assay analysis software (ANDOR Technology).

Histological Analysis. The embryonic gonads were fixed with 4% PFA overnight at 4 °C, and the adult mouse gonads were fixed with Bouin's solution overnight at 4 °C. The tissues fixed with Bouin's solution were washed on a shaker with 70% ethanol three times, and the tissues fixed with 4% PFA were washed on a shaker with PBS three times. Fixed samples were dehydrated with graded alcohol, embedded in paraffin, and cut into 5-μm-thick sections.

For hematoxylin and eosin staining, sections were deparaffinized, rehydrated, and stained with hematoxylin and eosin following a standard protocol. Images were captured under an Olympus microscope (BX53).

For immunohistochemistry, sections of gonads were deparaffinized, rehydrated, and boiled for 20 min with citrate buffer (pH 6.0) in a water bath for antigen retrieval. After cooling at room temperature, the slides were washed with distilled water twice, blocked, and permeabilized for 1 h at room temperature with 10% goat or donkey serum containing 0.3% Triton X-100. Slides were then incubated with the desired primary antibodies (*SI Appendix*, Table S2) at 4 °C overnight before they were washed three times with PBST and stained according to a standard procedure of the horse radish peroxidase-based immunohistochemistry using a Vectstain ABC Kit (Vector Laboratory). Thereafter, sections were counterstained with hematoxylin, dehydrated in a gradient series of ethanol, and treated with xylene twice to acquire more transparent visualization. Finally, slides were mounted with neutral balsam mounting medium and imaged under an Olympus microscope (BX53).

Alkaline Phosphatase Staining. Pregnant mice at E8.5∼E11.5 were killed, and embryos were collected, fixed in 4% PFA for 1 h at 4 °C, washed twice with PBS, and stained with freshly prepared staining buffer for 20∼30 min on a

shaker at 37 °C. The staining buffer was protected from light and prepared as follows: 25 mM Tris-maleic acid buffer (pH 9.0), 0.5 mM MgCl$_2$, 0.4 mg/mL 1-naphthyl phosphate disodium salt, and 1 mg/mL Fast Red TR salt (53). Staining was stopped by adding an excessive volume of PBS. Samples were washed twice with ddH$_2$O and cleared with 40% glycerol and 80% glycerol for 1 h. Images were captured under a stereoscope (Nikon).

Vectors, chemicals, and reagents used in this study are listed in *SI Appendix*, Table S3.

Quantification and Statistical Analysis. The data were collected and analyzed in a blinded manner. Generally, 300∼800 cells or 5∼16 embryos were included for statistical analysis. The sample sizes are presented in the figure legends. Most of the experiments were repeated approximately three to five independent times. GraphPad Prism v8.0c was used for graphics construction and statistical analysis. Two-tailed P values were obtained using Student's t test and the difference was considered to be statistically significant when $P < 0.05$.

Data, Materials, and Software Availability. All study data are available in the article and/or supporting information. Deposited data from an external source are not used.

Author affiliations: ᵃCenter for Reproductive Medicine, Cheeloo College of Medicine, Shandong University, Jinan, 250012, China; ᵇKey Laboratory of Reproductive Endocrinology of Ministry of Education, Shandong University, Jinan, 250012, China; ᶜShandong Key Laboratory of Reproductive Medicine, Jinan, 250012, China; ᵈShandong Provincial Clinical Research Center for Reproductive Health, Jinan, 250012, China; ᵉNational Research Center for Assisted Reproductive Technology and Reproductive Genetics, Shandong University, Jinan, 250012, China; ᶠState Key Laboratory of Genetic Resources and Evolution, Kunming Institute of Zoology, Chinese Academy of Sciences, Kunming, 650223, China; ᵍYunnan Key Laboratory of Animal Reproduction, Kunming Institute of Zoology, Chinese Academy of Sciences, Kunming, 650223, China; ʰState Key Laboratory of Stem Cell and Reproductive Biology, Institute of Zoology, Chinese Academy of Sciences, Beijing, 100101, China; ⁱUniversity of Chinese Academy of Sciences, Beijing, 100101, China; ʲResearch Unit of Gametogenesis and Health of ART-Offspring, Chinese Academy of Medical Sciences,China; ᵏShanghai Key Laboratory for Assisted Reproduction and Reproductive Genetics, Shanghai, 200135, China; and ˡCenter for Reproductive Medicine, Ren Ji Hospital, School of Medicine, Shanghai Jiao Tong University, Shanghai, 200135, China

1. M. Saitou, M. Yamaji, Primordial germ cells in mice. *Cold Spring Harb. Perspect. Biol.* **4**, a008375 (2012).
2. P. Murphey, D. J. McLean, C. A. McMahan, C. A. Walter, J. R. McCarrey, Enhanced genetic integrity in mouse germ cells. *Biol. Reprod.* **88**, 6 (2013).
3. B. Milholland et al., Differences between germline and somatic mutation rates in humans and mice. *Nat. Commun.* **8**, 15183 (2017).
4. V. D. Rinaldi, E. Bolcun-Filas, H. Kogo, H. Kurahashi, J. C. Schimenti, The DNA damage checkpoint eliminates mouse oocytes with chromosome synapsis failure. *Mol. Cell* **67**, 1026–1036.e2 (2017).
5. E. K. Suh et al., p63 protects the female germ line during meiotic arrest. *Nature* **444**, 624–628 (2006).
6. V. Tsui, W. Crismani, The Fanconi anemia pathway and fertility. *Trends Genet.* **35**, 199–214 (2019).
7. S. Messiaen et al., Rad54 is required for the normal development of male and female germ cells and contributes to the maintainance of their genome integrity after genotoxic stress. *Cell Death Dis.* **4**, e774 (2013).
8. Y. Luo, J. C. Schimenti, MCM9 deficiency delays primordial germ cell proliferation independent of the ATM pathway. *Genesis* **53**, 678–684 (2015).
9. R. J. Hill, G. P. Crossan, DNA cross-link repair safeguards genomic stability during premeiotic germ cell development. *Nat. Genet.* **51**, 1283–1294 (2019).
10. S. Kagiwada, K. Kurimoto, T. Hirota, M. Yamaji, M. Saitou, Replication-coupled passive DNA demethylation for the erasure of genome imprints in mice. *EMBO J.* **32**, 340–353 (2013).
11. M. Per<charde, P. Wong, M. Ramalho-Santos, Global hypertranscription in the mouse embryonic germline. *Cell Rep.* **19**, 1987–1996 (2017).
12. S. Hamperl, K. A. Cimprich, Conflict resolution in the genome: How transcription and replication make it work. *Cell* **167**, 1455–1467 (2016).
13. B. Gómez-González, A. Aguilera, Transcription-mediated replication hindrance: A major driver of genome instability. *Genes Dev.* **33**, 1008–1026 (2019).
14. M. P. Crossley, M. Bocek, K. A. Cimprich, R-loops as cellular regulators and genomic threats. *Mol. Cell* **73**, 398–411 (2019).
15. L. J. Mah, A. El-Osta, T. C. Karagiannis, gammaH2AX: A sensitive molecular marker of DNA damage and repair. *Leukemia* **24**, 679–686 (2010).
16. I. M. Ward, J. Chen, Histone H2AX is phosphorylated in an ATR-dependent manner in response to replicational stress. *J. Biol. Chem.* **276**, 47759–47762 (2001).

17. M. K. Zeman, K. A. Cimprich, Causes and consequences of replication stress. *Nat. Cell Biol.* **16**, 2–9 (2014).
18. R. A. Schwab *et al.*, The Fanconi anemia pathway maintains genome stability by coordinating replication and transcription. *Mol. Cell* **60**, 351–361 (2015).
19. T. García-Muse, A. Aguilera, Transcription-replication conflicts: How they occur and how they are resolved. *Nat. Rev. Mol. Cell Biol.* **17**, 553–563 (2016).
20. L. Guitton-Sert, Y. Gao, J. Y. Masson, Animal models of Fanconi anemia: A developmental and therapeutic perspective on a multifaceted disease. *Semin. Cell Dev. Biol.* **113**, 113–131 (2021).
21. R. Che, J. Zhang, M. Nepal, B. Han, P. Fei, Multifaceted Fanconi anemia signaling. *Trends Genet.* **34**, 171–183 (2018).
22. S. van Twest *et al.*, Mechanism of ubiquitination and deubiquitination in the Fanconi anemia pathway. *Mol. Cell* **65**, 247–259 (2017).
23. A. Smogorzewska *et al.*, Identification of the FANCI protein, a monoubiquitinated FANCD2 paralog required for DNA repair. *Cell* **129**, 289–301 (2007).
24. M. Ishiai *et al.*, FANCI phosphorylation functions as a molecular switch to turn on the Fanconi anemia pathway. *Nat. Struct. Mol. Biol.* **15**, 1138–1146 (2008).
25. T. Shigechi *et al.*, ATR-ATRIP kinase complex triggers activation of the Fanconi anemia DNA repair pathway. *Cancer Res.* **72**, 1149–1156 (2012).
26. L. Xu *et al.*, FANCI plays an essential role in spermatogenesis and regulates meiotic histone methylation. *Cell Death Dis.* **12**, 780 (2021).
27. H. Liao, F. Ji, T. Helleday, S. Ying, Mechanisms for stalled replication fork stabilization: New targets for synthetic lethality strategies in cancer treatments. *EMBO Rep.* **19**, e46263 (2018).
28. Z. Liang *et al.*, Binding of FANCI-FANCD2 complex to RNA and R-loops stimulates robust FANCD2 monoubiquitination. *Cell Rep.* **26**, 564–572.e5 (2019).
29. K. Schlacher, H. Wu, M. Jasin, A distinct replication fork protection pathway connects Fanconi anemia tumor suppressors to RAD51-BRCA1/2. *Cancer Cell* **22**, 106–116 (2012).
30. H. Gaillard, A. Aguilera, Transcription as a threat to genome integrity. *Annu. Rev. Biochem.* **85**, 291–317 (2016).
31. Y. Seki *et al.*, Cellular dynamics associated with the genome-wide epigenetic reprogramming in migrating primordial germ cells in mice. *Development* **134**, 2627–2638 (2007).
32. A. Panagopoulos, M. Altmeyer, The hammer and the dance of cell cycle control. *Trends Biochem. Sci.* **46**, 301–314 (2021).
33. R. Ceccaldi *et al.*, Bone marrow failure in Fanconi anemia is triggered by an exacerbated p53/p21 DNA damage response that impairs hematopoietic stem and progenitor cells. *Cell Stem Cell* **11**, 36–49 (2012).
34. Y. Luo *et al.*, Hypersensitivity of primordial germ cells to compromised replication-associated DNA repair involves ATM-p53-p21 signaling. *PLoS Genet.* **10**, e1004471 (2014).
35. T. Otto, P. Sicinski, Cell cycle proteins as promising targets in cancer therapy. *Nat. Rev. Cancer* **17**, 93–115 (2017).
36. J. C. Bloom, J. C. Schimenti, Sexually dimorphic DNA damage responses and mutation avoidance in the mouse germline. *Genes Dev.* **34**, 1637–1649 (2020).
37. H. G. Leitch, W. W. Tang, M. A. Surani, Primordial germ-cell development and epigenetic reprogramming in mammals. *Curr. Top. Dev. Biol.* **104**, 149–187 (2013).
38. A. D. Auerbach, Fanconi anemia and its diagnosis. *Mutat. Res.* **668**, 4–10 (2009).
39. E. L. Dubois *et al.*, A Fanci knockout mouse model reveals common and distinct functions for FANCI and FANCD2. *Nucleic Acids Res.* **47**, 7532–7547 (2019).
40. P. Kotsantis *et al.*, Increased global transcription activity as a mechanism of replication stress in cancer. *Nat. Commun.* **7**, 13087 (2016).
41. M. Macheret, T. D. Halazonetis, Intragenic origins due to short G1 phases underlie oncogene-induced DNA replication stress. *Nature* **555**, 112–116 (2018).
42. C. Domenech *et al.*, Studies in an early development window unveils a severe HSC defect in both murine and human Fanconi anemia. *Stem Cell Reports* **11**, 1075–1091 (2018).
43. D. Walter *et al.*, Exit from dormancy provokes DNA-damage-induced attrition in haematopoietic stem cells. *Nature* **520**, 549–552 (2015).
44. L. U. Müller *et al.*, Overcoming reprogramming resistance of Fanconi anemia cells. *Blood* **119**, 5449–5457 (2012).
45. T. M. Chlon *et al.*, Overcoming pluripotent stem cell dependence on the repair of endogenous DNA damage. *Stem Cell Reports* **6**, 44–54 (2016).
46. M. Percharde, A. Bulut-Karslioglu, M. Ramalho-Santos, Hypertranscription in development, stem cells, and regeneration. *Dev. Cell* **40**, 9–21 (2017).
47. V. S. Vanni *et al.*, The neglected members of the family: Non-BRCA mutations in the Fanconi anemia/BRCA pathway and reproduction. *Hum. Reprod. Update* **28**, 296–311 (2022).
48. K. S. Ruth *et al.*; Biobank-based Integrative Omics Study (BIOS) Consortium; eQTLGen Consortium; Biobank Japan Project; China Kadoorie Biobank Collaborative Group; kConFab Investigators; LifeLines Cohort Study; InterAct consortium; 23andMe Research Team, Genetic insights into biological mechanisms governing human ovarian ageing. *Nature* **596**, 393–397 (2021).
49. Z. Lin *et al.*, Mettl3-/Mettl14-mediated mRNA N^6-methyladenosine modulates murine spermatogenesis. *Cell Res.* **27**, 1216–1230 (2017).
50. K. Morohaku *et al.*, Complete in vitro generation of fertile oocytes from mouse primordial germ cells. *Proc. Natl. Acad. Sci. U.S.A.* **113**, 9021–9026 (2016).
51. R. A. Schwab, W. Niedzwiedz, Visualization of DNA replication in the vertebrate model system DT40 using the DNA fiber technique. *J. Vis. Exp.* **56**, e3255 (2011).
52. U. Swain, K. Subba Rao, Study of DNA damage via the comet assay and base excision repair activities in rat brain neurons and astrocytes during aging. *Mech. Ageing Dev.* **132**, 374–381 (2011).
53. J. E. Cooke, I. Godin, C. Ffrench-Constant, J. Heasman, C. C. Wylie, Culture and manipulation of primordial germ cells. *Methods Enzymol.* **225**, 37–58 (1993).